JJEE
Volume 6, Number 2, 2020
Pages 110-127
Jordan Journal of Electrical Engineering
ISSN (Print): 2409-9600, ISSN (Online): 2409-9619

A DMWT-Based Relaying Scheme for the Recognition of Shunt Faults in a Two-Terminal Series Capacitor Compensated Transmission Line

Shyam Sunder Gupta[1], Gaurav Kapoor[2*], Jinendra Rahul[3]

[1, 3] Department of Electrical Engineering, Swami Keshvanand Institute of Technology, Management and Gramothan, Jaipur, India
[2] Department of Electrical Engineering, Modi Institute of Technology, Kota, India
E-mail: gaurav.kapoor019@gmail.com

Received: December 27, 2019 *Revised: January 24, 2020* *Accepted: February 5, 2020*

***Abstract*—** This paper proposes a discrete Meyer wavelet transform (DMWT)-based fault recognition and faulty phase categorization technique for the protection of two-terminal series capacitor compensated transmission line (TTSCCTL). The captured single side fault currents of the TTSCCTL are used to evaluate the amplitudes of DMWT coefficients at fifth level. To validate the performance of the proposed technique; a widespread collection of simulation studies are conducted with varied fault type, location, resistance, frequency, and switching time. In this work, the value of fault resistance is varied from 0.5 Ω to 105 Ω; the position of fault for the close-in relay faults is varied from 5 km to 9 km; the position of fault for the far-end relay faults is varied from 195 km to 199 km; the position of fault around the series capacitors are changed; the degree of series compensation is also varied from 15% to 70%; the performance of DMWT is also investigated for intense loads connection and the frequency of TTSCCTL is also varied from 48 Hz to 52 Hz. The obtained results show that DMWT correctly detects all types of faults in TTSCCTL by employing one-side fault current data only. They also proved that the proposed technique is robust to the variation in the fault factors of TTSCCTL.

***Keywords*—** Discrete Meyer wavelet transform; Fault recognition; Fault phase categorization; Three-phase series compensated transmission line protection.

1. INTRODUCTION

Among the different components of power transmission and distribution systems, transmission lines are most expected to experience faults. Therefore, it is vital to protect them. Recognition of faults in transmission lines is essential to provide adept and regular power flow. Many researchers proposed different techniques for the detection and classification of transmission lines' faults. In the recent years, wavelet transform has been effectively tested - by many researchers - for the transmission line protection. Series compensation of transmission line using series capacitors not only compensate the inductive reactance of the transmission line but also enhances its power transfer competence.

Several newly reported research works addressed the issue related to fault recognition and categorization in two-terminal series capacitor compensated transmission lines (TTSCCTL). Some important research works are presented here concisely. A combination of discrete Fourier transform (DFT) and fuzzy logic (FL) has been used to detect fault and select the faulty phase in 735 kV, 400 km long series compensated transmission line; the authors detected the faults within one cycle of power frequency [1]. A fault detection and classification scheme during power swing using maximum overlap discrete wavelet transform (MODWT) is reported [2]. An intrusion detection algorithm using line current differential relays has been tested on IEEE-14 bus and IEEE-39 bus networks [3]. Variational

* Corresponding author
Article's DOI: 10.5455/jjee.204-1581015688

mode decomposition and Hilbert transform based protection technique have been applied for micro-grid differential protection [4]. Further, the fault is detected on a 765 kV and 200 km long transmission line using harmonic wavelet transform and decision tree (DT) [5]. A convolutional neural network based relaying technique has been proposed for a 34.5 kV, 60 Hz PV fed micro-grid network [6]. Fault classification has been carried out in a 750 kV transmission line using discrete wavelet transform [7]. Using ensemble of decision tree; fault detection and classification have been carried out on a 400 kV and 200 km double circuit transmission line model [8]. An artificial neural network has been used for fault classification in double fed induction generator, connected to the grid using long transmission lines [9]. Fuzzy logic based relaying scheme has been presented to detect faults in an IEC 61850-7-420 micro-grid model of 120 kV and 60 Hz [10]. The DT aided travelling wave based fault detection, fault classification, fault location and faulty section identification techniques have been presented for multi-terminal transmission lines [11]. The protection technique for high impedance fault detection and classification in unified power flow controller (UPFC) compensated 400 km long, 400 kV and 50 Hz double circuit transmission line (DCTL) has been described [12]. A scheme based on parameter optimized variational mode decomposition and weighted P-norm random vector functional link network for fault location in a 400 kV, 50 Hz and 300 km long thyristor controlled series capacitor connected series compensated DCTL has been presented [13].

In this work, a discrete Meyer wavelet transform (DMWT)-based technique is proposed - for the recognition of faults and categorization of faulty phase in the TTSCCTL - and its competency in recognizing the faults, regardless of the deviations in the fault factors is investigated.

This article is structured as follows: Section 2 presents the specifications of TTSCCTL, Section 3 describes the process of fault recognition and faulty phase categorization using DMWT, Section 4 presents the simulation results and discussions and Section 5 concludes the article.

2. DESCRIPTION OF TWO-TERMINAL SERIES COMPENSATED TRANSMISSION LINE

The DMWT-based fault recognition technique has been executed on a 400 kV three-phase and 50 Hz series capacitor compensated transmission line of 200 km long. Fig. 1 shows the schematic of the proposed network. A 400 kV power source is connected at both terminals of the transmission line. The TTSCCTL is alienated into two zones of 100 km long each. The current measuring devices are installed at bus-1 (relaying point) of the TTSCCTL. To execute the simulations, this 400 kV TTSCCTL has been designed and simulated for various types of faults using MATLAB software. For each and every fault case, the fault factors are varied in order to investigate the impact of varying the fault factors on the performance of the proposed DMWT-based fault recognition technique. The value of fault resistance is varied from 0.5 Ω to 105 Ω; the position of fault for the close-in relay faults is varied from 5 km to 9 km; the position of fault for the far-end relay faults is varied from 195 km to 199 km; the position of fault around the series capacitors are changed; the degree of series compensation is also varied from 15% to 70%. The performance of DMWT has also been investigated for intense loads' connection and the frequency of TTSCCTL is also varied

from 48 Hz to 52 Hz. In this work, the TTSCCTL has been simulated for various types of phase to phase and phase to ground faults.

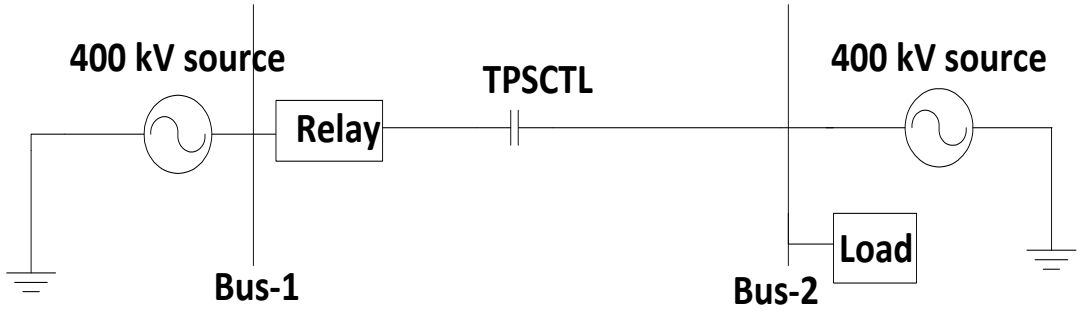

Fig. 1. Schematic of the 400 kV TTSCCTL.

3. DMWT-BASED FAULT RECOGNITION AND FAULTY PHASE CATEGORIZATION TECHNIQUE

The wavelet and scaling functions of Meyer wavelet are defined in the frequency domain because of its attractive features like accuracy and simplicity. Then; they are used for the detecting, classifying and locating faults in the transmission line. Using different decomposition levels; features of the fault transient disturbances can be easily obtained.

The wavelet and the scaling functions are defined in Eqs. (1) and (2), respectively as:

$$\psi^{\wedge}(\omega) = (2\pi)^{\wedge} - 1/2 \bullet e^{\wedge}\, j\omega/2 \bullet \sin\left(\frac{\pi}{2}\upsilon\left(\frac{3}{2\pi}|\omega| - 1\right)\right) \quad (1)$$

$$\phi^{\wedge}(\omega) = (2\pi)^{\wedge} - 1/2 \quad (2)$$

where Ψ is the wavelet function, Φ is the scaling function and ν is the auxiliary function of Meyer wavelet.

In this work, DMWT is utilized because it decomposes the fault currents into finite impulse response approximate, details coefficients at different decomposition levels and has many advantages over the other fault detection tools. Fig. 2 illustrates the process for the proposed DMWT-based fault recognition technique. The steps are stated as:

- Step 1: simulating the TTSCCTL in order to create faults and record the post-fault currents and zero sequence component of current. The zero sequence current is recorded because it is used for the recognition of ground faults.
- Step 2: applying DMWT on phases-A, B, and C and on zero sequence current to examine the post-fault currents for characteristics retrieval. The amplitude of DMWT coefficients is then evaluated.
- Step 3: selecting a common threshold value for all of faults' cases. In this work, a common threshold value of 1000 is selected after carrying out extensive simulation studies.
- Step 4: proclaiming the phase as the faulty phase and the relay will issue the trip signal when the DMWT output of the three-phase currents exceeds the threshold value; else there will be no-fault in the TTSCCTL.

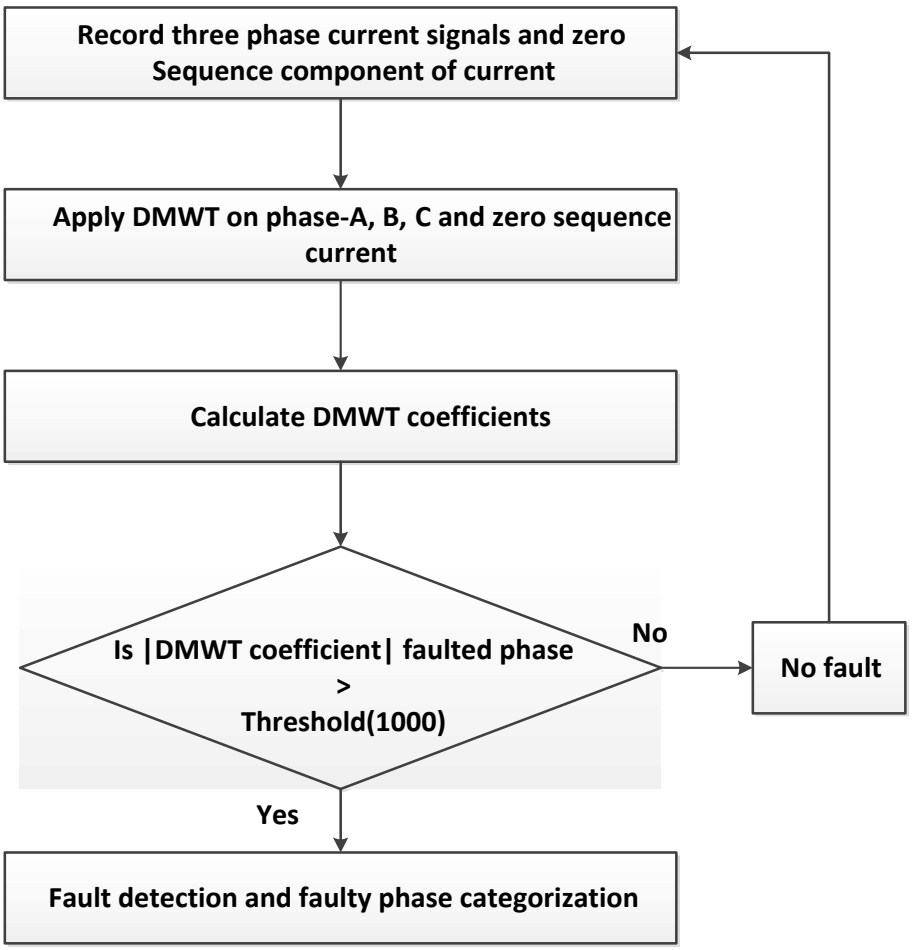

Fig. 2. The procedure of fault recognition using DMWT.

4. SIMULATION RESULTS AND DISCUSSION

The performance of the proposed DMWT-based technique has been investigated for different types of grounded and un-grounded faults under various fault factors such as fault resistance (R_F), ground resistance (R_G), fault switching time (FST) and fault location of (F_L). In this work, the value of fault resistance is varied from 0.5 Ω to 105 Ω, and the location of fault is varied from 5 km to 9 km for close-in relay faults and from 195 km to 199 km for far-end relay faults. The results of the work are presented in the next subsections.

4.1. Effectiveness of DMWT During Healthy Situation

The proposed DMWT-based technique has been investigated for a healthy situation of the transmission line. Fig. 3 exhibits the three-phase currents and voltages for no-fault situation and Fig. 4 depicts the DMWT output of three-phase currents for no-fault situation. From Fig. 4, it is observed that the DMWT coefficients of three-phase currents during no-fault situation are beneath the threshold line which means that the three-phase series compensated transmission line has no-fault. The amplitudes of DMWT coefficients of three-phase currents for no-fault situation are shown in Table 1. It is clear that the three-phase transmission line has no-fault as the amplitudes are less than the threshold value of 1000.

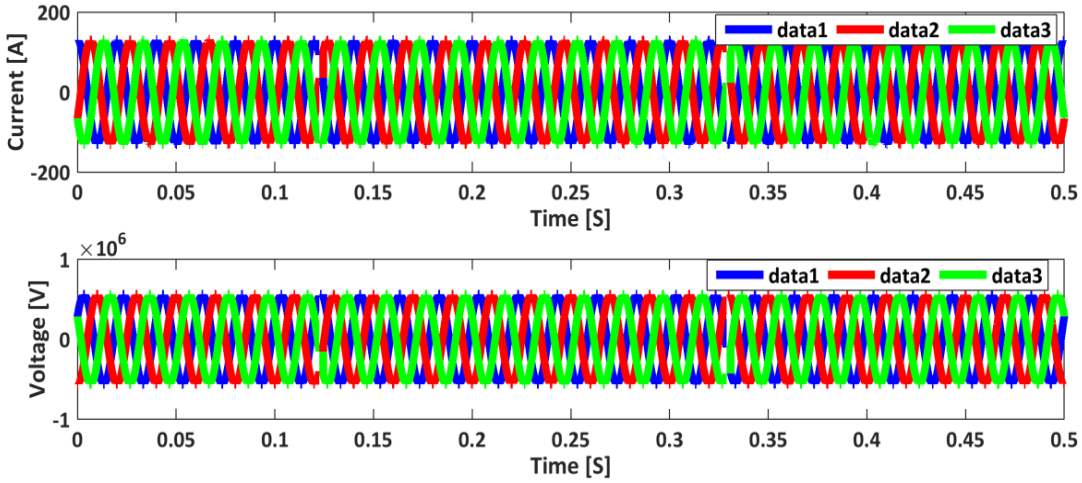

Fig. 3. Three-phase currents and voltages during no-fault.

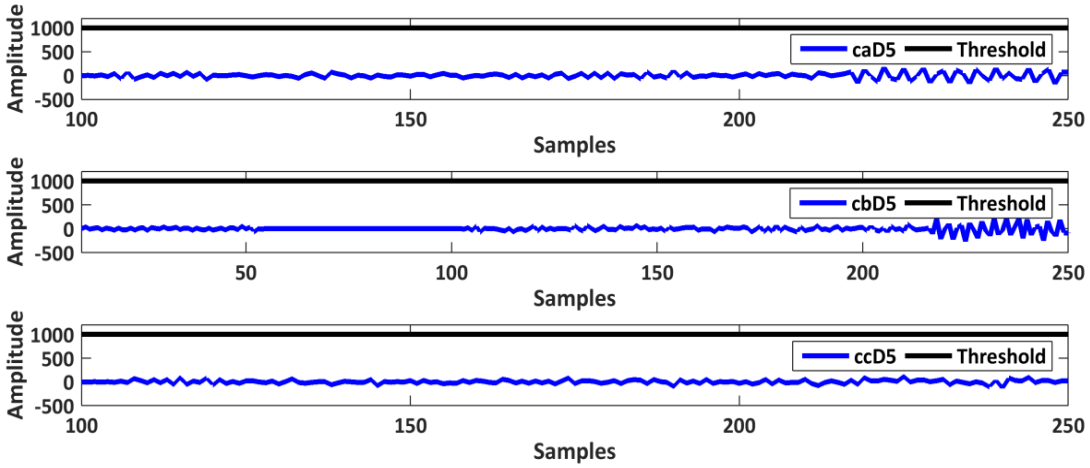

Fig. 4. DMWT coefficients of three-phase currents during no-fault.

Table 1. Amplitudes of DMWT coefficients of three-phase currents for no-fault situation.

DMWT outputs				Relay output
Phase-A	Phase-B	Phase-C	Ground	
182.7194	235.2369	111.1152	4.6755*10^-8	No-Fault

4.2. Effectiveness of DMWT in Detecting Different Fault Types

The performance of DMWT has been investigated for different types of grounded and ungrounded faults simulated on TTSCCTL. Fig. 5 depicts the three-phase currents for a single-phase to ground AG fault tested at 100 km and 0.05 s with R_F = 1.25 Ω and R_G = 2.15 Ω. Fig. 6 exemplifies the output of DMWT as coefficients of three-phase currents during AG fault in which the DMWT coefficient of phase-A crosses the threshold nearly at sample#130, and the coefficients of all other phases stay below the threshold line; evidently signifying the occurrence of AG fault on TTSCCTL. The fault factors - selected here for all the fault cases - are: F_L = 100 km; FST = 0.05 s; R_F = 1.25 Ω and R_G = 2.15 Ω. Table 2 reports the results of the proposed DMWT-based scheme for different fault types. It is clear that the DMWT has the capability of detecting and classifying both grounded and ungrounded faults, simulated on the TTSCCTL.

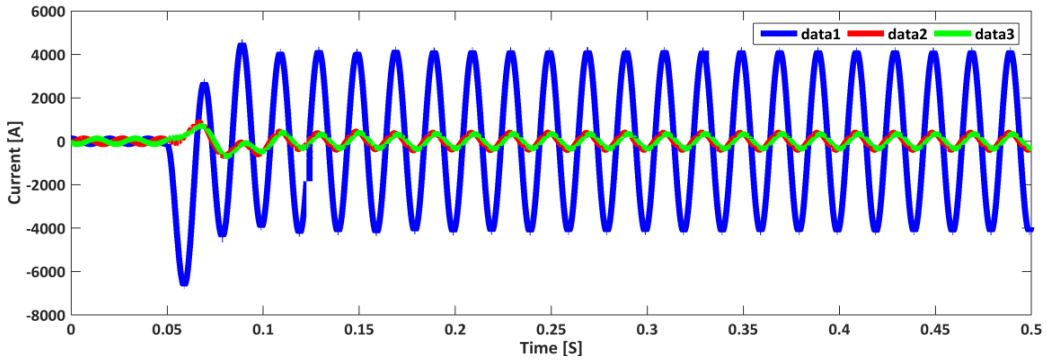

Fig. 5. AG fault at 100 km and 0.05 s with R_F = 1.25 Ω and R_G = 2.15 Ω.

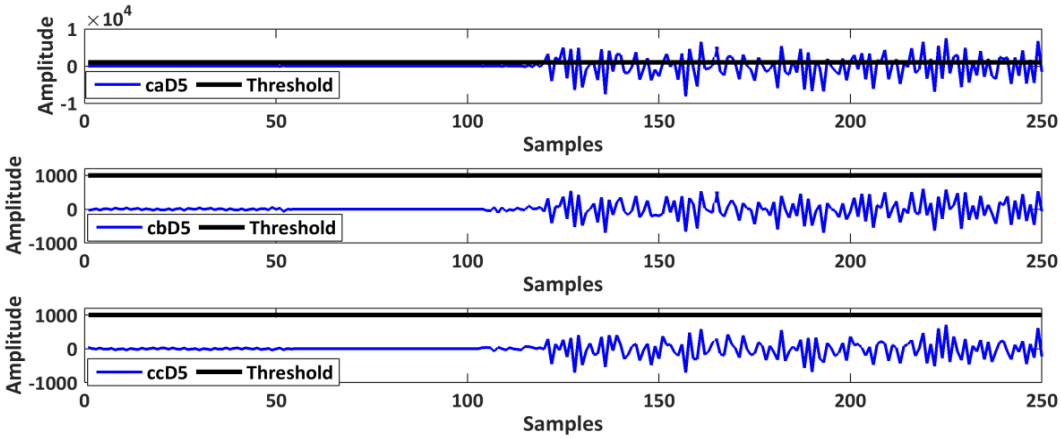

Fig. 6. DMWT coefficients during AG fault at 100 km and 0.05 s with R_F = 1.25 Ω and R_G = 2.15 Ω.

Table 2. Effectiveness of DMWT in detecting different grounded and ungrounded faults.

Fault type	R_F [Ω]	R_G [Ω]	FST [S]	F_L [km]	DMWT output				Relay output
					Phase-A	Phase-B	Phase-C	Ground	
AG	1.25	2.15	0.05	100	7.5097*10^3	602.3038	713.8800	2.9361*10^3	AG
BG	1.25	2.15	0.05	100	713.6183	7.5810*10^3	704.3044	2.9624*10^3	BG
CG	1.25	2.15	0.05	100	968.5545	978.5123	9.1018*10^3	3.5572*10^3	CG
ABG	1.25	2.15	0.05	100	7.5750*10^3	7.0971*10^3	663.0465	704.6808	ABG
BCG	1.25	2.15	0.05	100	137.4490	8.0447*10^3	7.1294*10^3	701.4078	BCG
ACG	1.25	2.15	0.05	100	6.7151*10^3	593.3081	7.4094*10^3	817.7989	ACG
AB	1.25	2.15	0.05	100	1.2405*10^4	1.0276*10^4	159.3020	0.2674	AB
BC	1.25	2.15	0.05	100	146.6654	1.1938*10^4	1.2993*10^4	0.0828	BC
AC	1.25	2.15	0.05	100	1.0492*10^4	158.0134	4.2399*10^3	0.0944	AC
ABCG	1.25	2.15	0.05	100	9.5315*10^3	1.1249*10^4	6.1594*10^3	3.2382	ABCG
ABC	1.25	2.15	0.05	100	8.8331*10^3	1.2243*10^4	5.9548*10^3	95.2426	ABC

4.3. Effectiveness of DMWT in Detecting Faults Tested with Different Fault Resistances

The R_F causes mal-operation of various distance relays in the case of grounded faults. Hence; the influence of R_F on the performance of DMWT has been inspected for different values of R_F. Fig. 7 depicts the three-phase currents for the most rigorous fault: three-phase ABC fault simulated without ground at 100 km and 0.07 s with R_F = 0.5 Ω and R_G = 0.01 Ω. Fig. 8 exhibits the fault recognition and faulty phase categorization output of DMWT in which the amplitude of DMWT coefficients of all the phases A, B, and C are above the

threshold value; apparently signifying the incidence of ABC fault on TTSCCTL. The selected fault factors – which are common for all the fault cases - are: F_L = 100 km, FST = 0.07 s and R_G = 0.01 Ω. Table 3 reports the results of proposed scheme for different faults. It proves that the proposed DMWT-based technique effectively detects all types of faults - simulated on the TTSCCTL by varying the fault resistance - and categorizes the faulty phases as well. Thus; it is confirmed that the faults (with and without ground) with different fault resistances (lying between 0.5 Ω and 105 Ω) do not affect the performance of the proposed DMWT-based scheme.

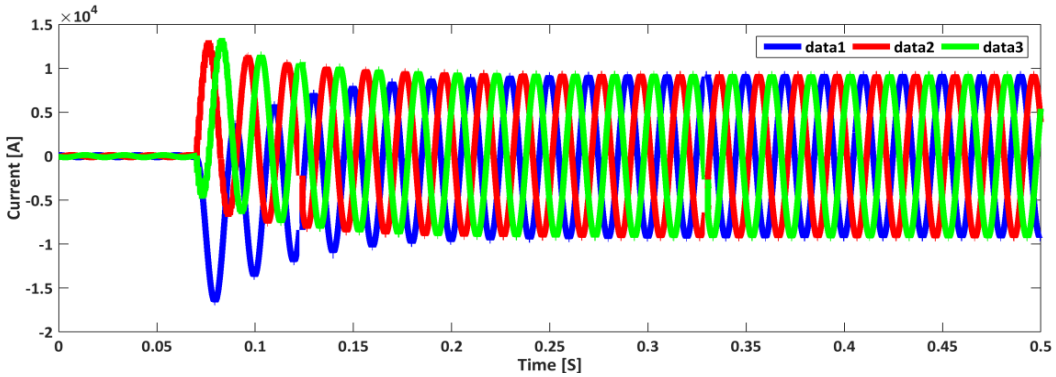

Fig. 7. ABC fault at 100 km and 0.07 s with R_F = 0.5 Ω and R_G = 0 Ω.

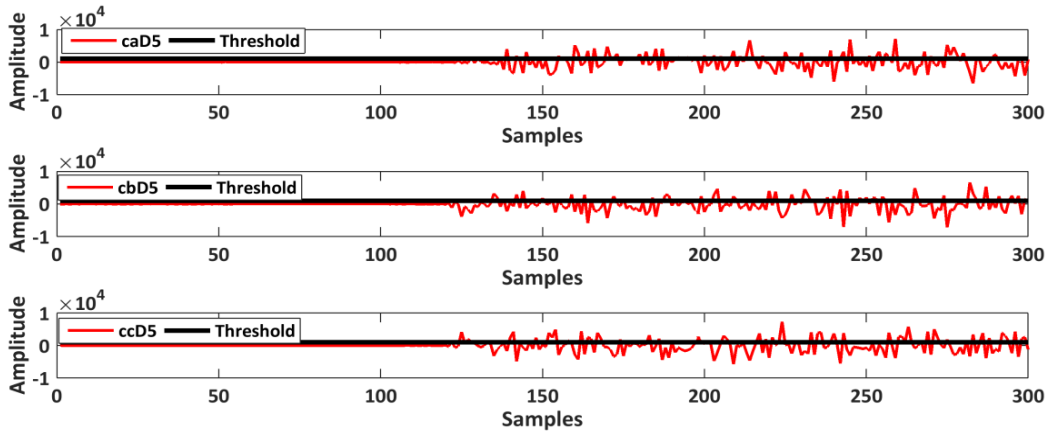

Fig. 8. DMWT coefficients of ABC fault current at 100 km and 0.07 s with R_F = 0.5 Ω and R_G = 0 Ω.

Table 3. Effectiveness of DMWT in detecting faults under different fault resistances.

Fault type	R_F [Ω]	R_G [Ω]	FST [s]	F_L [km]	DMWT output				O/P
					Phase-A	Phase-B	Phase-C	Ground	
ABC	0.5	0	0.07	100	7.2326*10^3	6.6237*10^3	1.0457*10^4	92.1734	ABC
BCG	15	0.01	0.07	100	310.8850	6.9496*10^3	4.7500*10^3	1.0952*10^3	BCG
AB	35	0.01	0.07	100	2.9720*10^3	3.3973*10^3	172.8492	0.0380	AB
ACG	75	0.01	0.07	100	3.3262*10^3	431.7913	2.0433*10^3	751.1873	ACG
BG	105	0.01	0.07	100	441.9002	3.3627*10^3	595.4893	1.3041*10^3	BG

4.4. Effectiveness of DMWT in Detecting Close-in Relay Faults

The consequence of close-in relay faults on the effectiveness of the DMWT-based technique has been investigated by varying the fault location from 5 km to 9 km. Fig. 9

depicts a case study of single-phase to ground AG near-in relay fault simulated at 5 km and 0.075 s with R_F = 1.75 Ω and R_G = 2.35 Ω. Fig. 10 shows the output of DMWT coefficients in which phase-A coefficients cross the threshold at sample#239 and all the other phases stay below the threshold line; undoubtedly pointing towards the occurrence of AG fault. The selected fault factors – which are common for all of the fault cases - are: FST = 0.075 s; R_F = 1.75 Ω and R_G = 2.35 Ω. Table 4 reports the results of the DMWT for different close-in relay faults. The simulation results - as reported in Table 4 - substantiate the effectiveness of DMWT for the recognition of near-in relay faults.

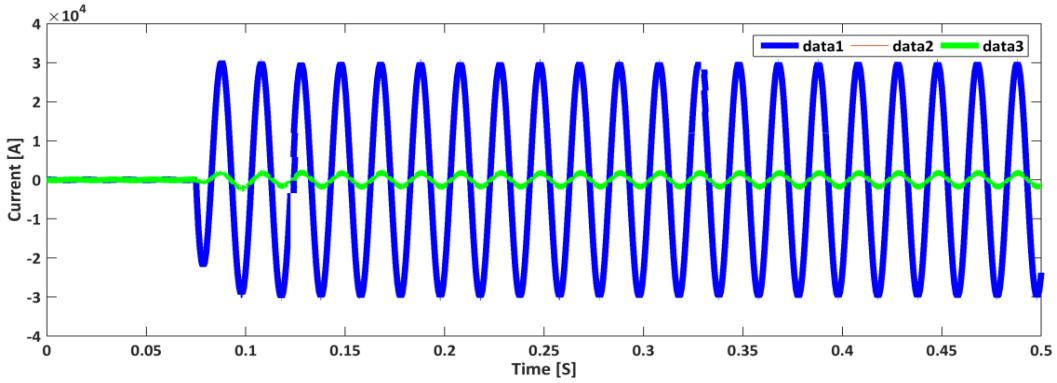

Fig. 9. AG close-in relay fault at 5 km and 0.075 s with R_F = 1.75 Ω and R_G = 2.35 Ω.

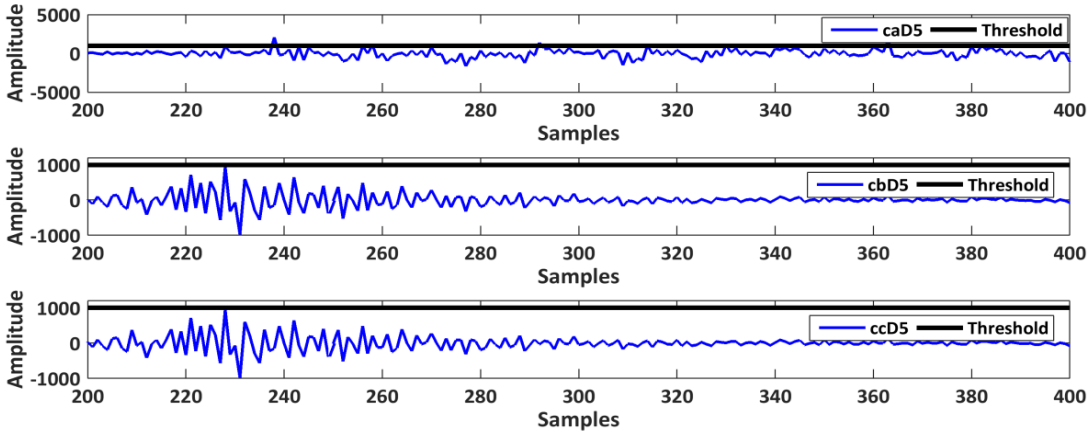

Fig. 10. DMWT coefficients for AG close-in relay fault at 5 km and 0.075 s with R_F = 1.75 Ω and R_G = 2.35 Ω.

Table 4. Effectiveness of DMWT in detecting the close-in relay faults.

Fault type	R_F [Ω]	R_G [Ω]	FST [s]	F_L [km]	DMWT output				Relay output
					Phase-A	Phase-B	Phase-C	Ground	
AG	1.75	2.35	0.075	5	2.0779*10^3	939.0050	939.0773	930.6080	AG
AC	1.75	2.35	0.075	6	3.3643*10^3	11.3378	3.6709*10^3	1.0002	AC
ABG	1.75	2.35	0.075	7	2.7003*10^3	3.6193*10^3	395.2035	505.9019	ABG
ABC	1.75	2.35	0.075	8	2.5309*10^3	4.2299*10^3	2.9471*10^3	38.0781	ABC
CG	1.75	2.35	0.075	9	367.1946	366.7707	3.4182*10^3	1.2747*10^3	CG

4.5. Effectiveness of DMWT in Detecting Far-end Relay Faults

The consequence of far-end relay faults on the effectiveness of the DMWT-based technique has been explored by varying the fault location from 195 km to 199 km. Fig. 11 presents a case study of phase to phase AB far-end relay fault simulated at 195 km and 0.08 s

with R_F = 3.5 Ω and R_G = 2.5 Ω. Fig. 12 shows the output of DMWT coefficients in which both phase-A and B coefficients cross the threshold at sample#70 and the coefficients of phase-C stay below the threshold line; indubitably indicating the occurrence of AB fault. The selected fault factors – which are common for all the fault cases are: FST = 0.08 s; R_F = 3.5 Ω and R_G = 2.5 Ω. Table 5 presents the results of the proposed scheme detection of different far-end relay faults. They prove that the proposed DMWT-based technique has the ability to detect the far-end relay faults and categorize the faulty phases perfectly.

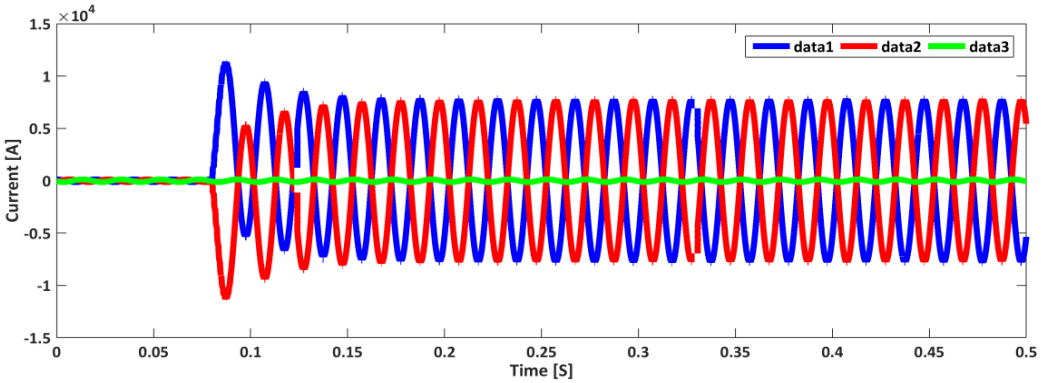

Fig. 11. AB far-end relay fault at 195 km and 0.08 s with R_F = 3.5 Ω and R_G = 0 Ω.

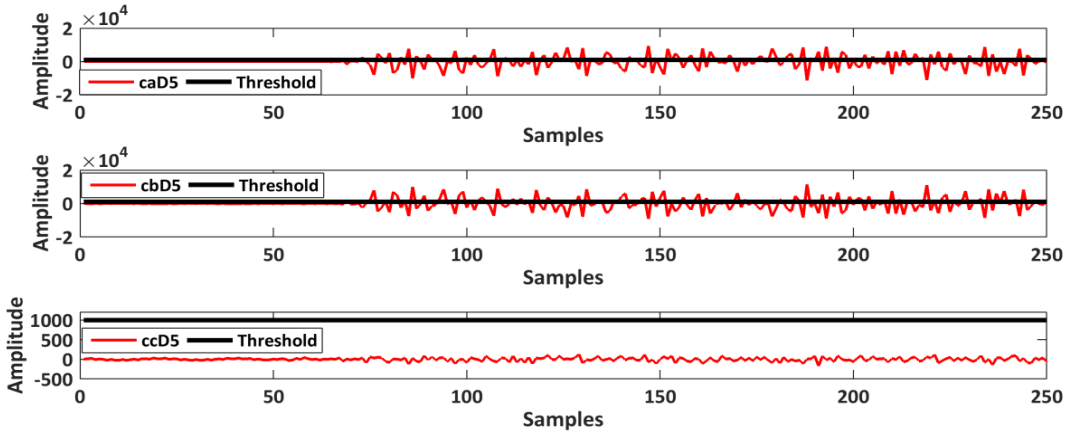

Fig. 12. DMWT coefficients for AB far-end relay fault at 195 km and 0.08 s with R_F = 3.5 Ω and R_G = 0 Ω.

Table 5. Effectiveness of DMWT in detecting the far-end relay faults.

Fault type	R_F [Ω]	R_G [Ω]	FST [s]	F_L [km]	DMWT output				Relay output
					Phase-A	Phase-B	Phase-C	Ground	
AB	3.5	0	0.08	195	1.0282*10^4	1.1420*10^4	158.5240	0.0837	AB
ABCG	3.5	2.5	0.08	196	6.1366*10^3	6.0665*10^3	6.1685*10^3	4.9297	ABCG
BCG	3.5	2.5	0.08	197	173.2490	7.5245*10^3	6.1789*10^3	662.1826	BCG
AG	3.5	2.5	0.08	198	7.5898*10^3	676.0762	659.0439	2.9205*10^3	AG
ABC	3.5	2.5	0.08	199	7.4557*10^3	6.8639*10^3	6.5113*10^3	94.9104	ABC

4.6. Effectiveness of DMWT in Detecting Evolving Faults

The potential of DMWT-based scheme has been tested for various types of evolving faults. An evolving fault is a type of fault wherein one fault type at a particular time is converted into another fault type at other different time. Fig. 13 depicts the three-phase

currents and the DMWT coefficients are presented in Fig. 14. Initially, BG fault has been simulated at 100 km and 0.05 s with R_F = 5 Ω and R_G = 0.01 Ω. This BG fault, after few cycles of current waveform, is converted into ABG fault at 100 km and 0.3 s with R_F = 10 Ω and R_G = 0.01 Ω. The fault selected factors are: F_L = 100 km and R_G = 0.01 Ω. The values of fault resistance, time and fault location are varied throughout the simulation studies of evolving faults. The switching time difference of both faults is 0.25 s. In Fig. 14, it is clearly seen that the DMWT coefficients of faulty phases A and B are above the threshold after FST while that of phase C are below the threshold. Table 6 reports the results of the proposed DMWT-based scheme for different evolving faults. They authenticate the competence of DMWT for the recognition of evolving faults. Moreover, the proposed scheme perfectly discriminates between the faulty and the healthy phase. From Table 6, it is evident that the evolving faults do not affect the performance of the proposed DMWT-based technique.

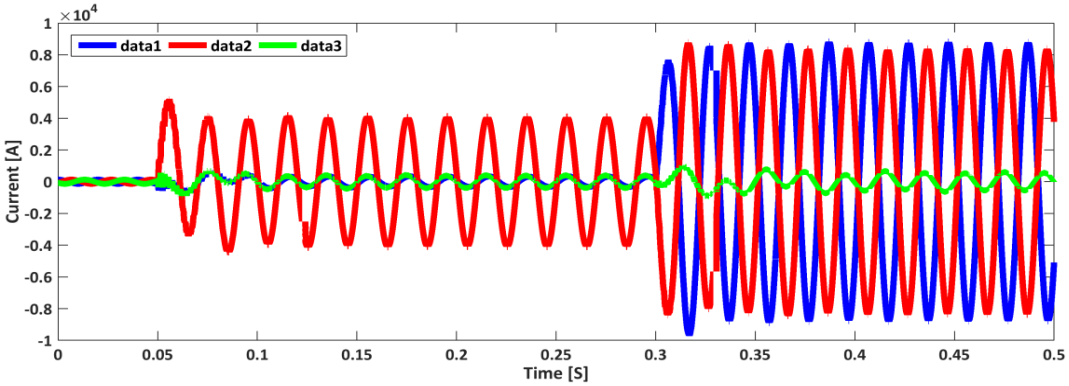

Fig. 13. The waveform with BG fault at 100 km and 0.05 s and with R_F= 5 Ω and R_G= 0.01 Ω, converted into ABG fault at 100 km and 0.3 s and with R_F= 10 Ω and R_G= 0.01 Ω.

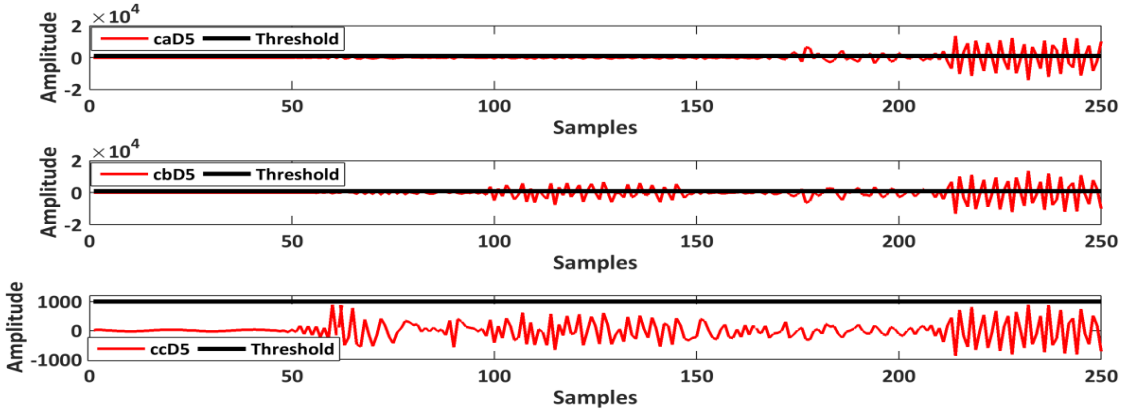

Fig. 14. DMWT coefficients with BG fault at 100 km and 0.05 s and with R_F= 5 Ω and R_G= 0.01 Ω, converted into ABG fault at 100 km and 0.3 s and with R_F= 10 Ω and R_G= 0.01 Ω.

Table 6. Effectiveness of DMWT in detecting the evolving faults.

FT-1	FT-2	R_{F1} [Ω]	R_{F2} [Ω]	T1 [s]	T2 [s]	T1-T2	F_{L1} [km]	F_{L2} [km]	DMWT output				O/P
									Phase-A	Phase-B	Phase-C	Ground	
BG	ABG	5	10	0.05	0.3	0.25	100	100	1.3653*10^4	1.3701*10^4	888.4112	2.6159*10^3	ABG
ABCG	AG	10	15	0.07	0.2	0.13	80	120	8.9637*10^3	7.4280*10^3	6.2352*10^3	2.7796*10^3	ABCG
CG	ABCG	15	20	0.08	0.315	0.235	130	70	9.9879*10^3	1.4962*10^4	8.2598*10^3	906.6360	ABCG
CG	ACG	20	25	0.055	0.3	0.245	75	125	7.8338*10^3	340.0223	9.3623*10^3	3.0065*10^3	ACG
BG	CG	25	30	0.09	0.25	0.16	120	80	931.2492	2.3634*10^3	7.4406*10^3	2.3221*10^3	BCG

4.7. Effectiveness of DMWT in Detecting Faults Around the Capacitors Bank

The feasibility of DMWT has also been investigated by performing various simulation studies after creating the faults around the bank of series capacitors on TTSCCTL. Sometimes, the conventional relays fail in detecting faults which occur before or after the position of series capacitors. Thus; it is very crucial to check the performance of the proposed technique for faults which occurs around the series capacitors. Fig. 15 shows a case study of LLG ACG fault simulated at 100 km and 0.1 s with R_F = 1.95 Ω and R_G = 2.65 Ω. Fig. 16 shows the output of DMWT coefficients in which both phase-A and C cross the threshold at sample#150 and the coefficients of phase-B stay below the threshold line; indubitably directing towards the incidence of ACG fault. The selected fault factors – which are common for all of the fault cases - are: FST = 0.1 s, R_F = 1.95 Ω and R_G = 2.65 Ω. Table 7 presents the results of the proposed scheme for various faults simulated around the bank of series capacitors on TTSCCTL. It proves that the DMWT-based has the ability to detect the faults occur around the bank of series capacitors and categorize the faulty phases effectively.

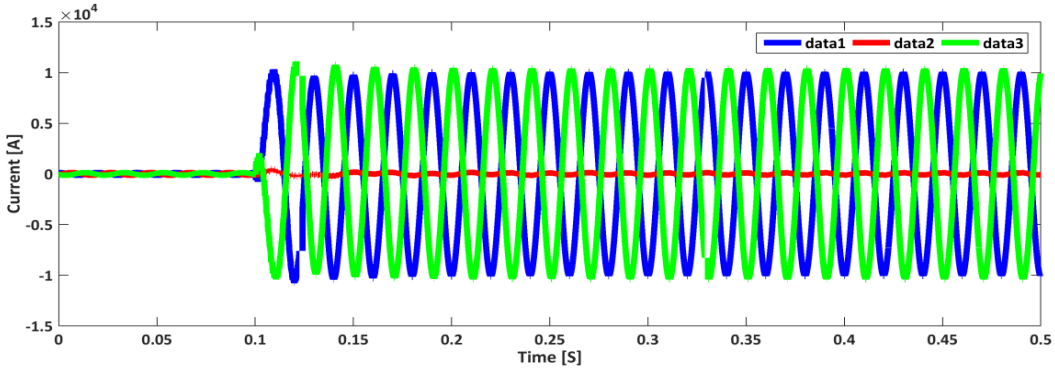

Fig. 15. ACG fault, simulated after the capacitor bank at 100 km and 0.1 s with R_F = 1.95 Ω and R_G = 2.65 Ω.

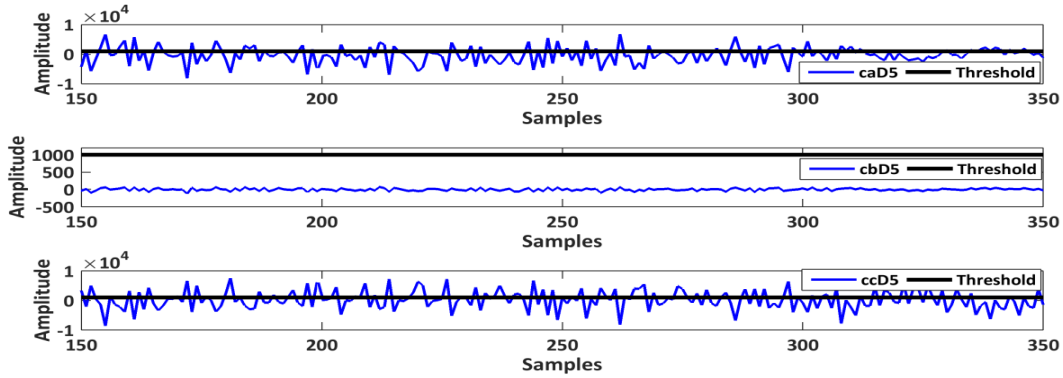

Fig. 16. DMWT coefficients for ACG fault, simulated after the capacitor bank, at 100 km and 0.1 s with R_F = 1.95 Ω and R_G = 2.65 Ω.

Table 7. Effectiveness of DMWT in detecting faults, simulated around the series capacitors.

F_T	FSP	R_F [Ω]	R_G [Ω]	FST [s]	F_L [km]	DMWT output				O/P
						Phase-A	Phase-B	Phase-C	Ground	
ACG	After	1.95	2.65	0.1	100	6.7961*10^3	602.8171	7.5689*10^3	1.5090*10^3	ACG
BG	Before	1.95	2.65	0.1	100	657.1988	8.0625*10^3	842.3912	3.1420*10^3	BG
AB	After	1.95	2.65	0.1	100	1.4609*10^4	1.5080*10^4	148.0080	0.2147	AB
AG	Before	1.95	2.65	0.1	100	7.6093*10^3	802.6739	612.6543	2.9368*10^3	AG
ABC	After	1.95	2.65	0.1	100	9.1967*10^3	8.1656*10^3	8.3169*10^3	89.1296	ABC

4.8. Effectiveness of DMWT in Detecting Faults with Various Levels of Series Compensation

The performance of the proposed DMWT-based technique has been explored by performing various test studies with variations in the degree of series compensation (%X) from 15% to 70%. Fig. 17 depicts the three-phase currents for a phase to phase AB fault tested with $\%X_C$ = 15% at 125 km and 0.1 s with R_F = 2.75 Ω and R_G = 1.75 Ω. Fig. 18 exemplifies the output of DMWT coefficients of three-phase currents during AB fault, in which phase-A and B coefficients cross the threshold nearly at sample#90 and the coefficient of phase C stays below the threshold line; evidently signifying the occurrence of AB fault on TTSCCTL. The selected fault factors – which are common for all of the fault cases - are: F_L = 125 km, FST = 0.1 s, R_F = 2.75 Ω and R_G = 1.75 Ω. Table 8 shows the results of the proposed DMWT-based scheme for different faults with different degrees of $\%X_C$. The results support the effectualness of DMWT under extensive variations in the degree of series compensation. Hence; the proposed DMWT-based technique provides excellent results for the recognition of faults and categorization of the faulty phases.

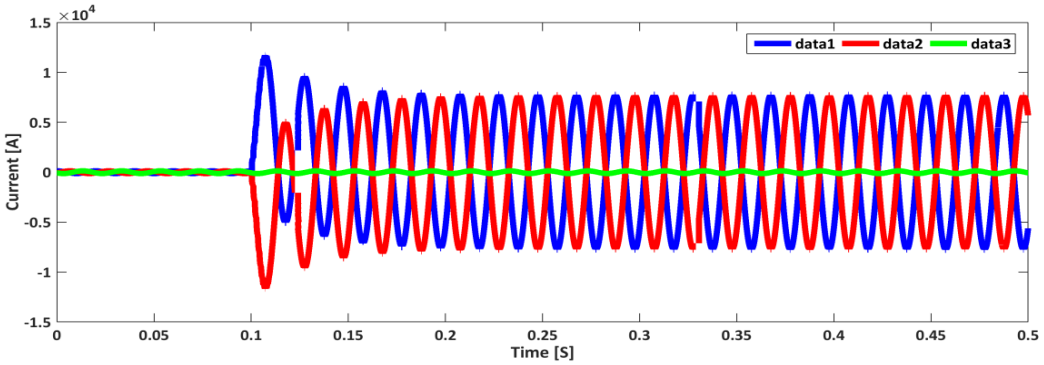

Fig. 17. AB fault at 125 km and 0.1 s with R_F = 2.75 Ω, R_G = 0 Ω and $\%X_C$ = 15%.

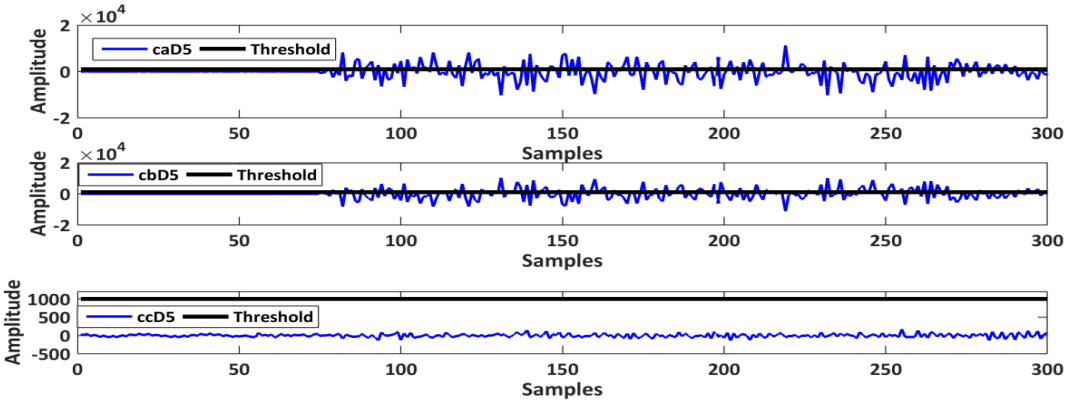

Fig. 18. DMWT coefficients for AB fault at 125 km and 0.1 s with R_F = 2.75 Ω, R_G = 0 Ω and $\%X_C$ = 15%.

Table 8. Effectiveness of DMWT in detecting faults with variations in the level of series compensation.

F_T	%X	R_F [Ω]	R_G [Ω]	FST [s]	F_L [km]	DMWT output				O/P
						Phase-A	Phase-B	Phase-C	Ground	
AB	15	2.75	0	0.1	125	1.1297*10^4	1.0332*10^4	172.9250	0.0949	AB
BCG	25	2.75	1.75	0.1	125	155.7531	3.1392*10^3	2.8797*10^3	312.2264	BCG
AG	35	2.75	1.75	0.1	125	2.4836*10^3	569.7634	480.1951	1.1145*10^3	AG
ABC	65	2.75	1.75	0.1	125	3.6233*10^3	4.8179*10^3	4.4539*10^3	109.1600	ABC
ACG	70	2.75	1.75	0.1	125	3.7868*10^3	731.0989	3.1200*10^3	398.6951	ACG

4.9. Effectiveness of DMWT in Detecting Faults during Intense-Load Interconnection

Persistently, the conventional relay declares the fault during an unexpected interconnection of load because it is not counted in any category of fault. Therefore, it is essential to test DMWT-based scheme performance for different intense loads interconnection. To achieve this goal a load having an active power P = 550 MW and a reactive power Q=350 MVAr, is connected with bus-2 (far-end point, at 200 km) at 0.1 s as depicted in Fig. 19. It shows the waveform of three-phase currents during a heavy load connection with TTSCCTL. It is evident that the current increases at T=0.1 s. Fig. 20 shows the fault recognition output of DMWT wherein the DMWT coefficients of all phases A, B, and C are below the threshold line; definitely directing towards no-fault in TTSCCTL during the intense load interconnection. Table 9 reports the results of the proposed DMWT-based scheme for interconnecting different types of intense loads with TTSCCTL. It is clear that the performance of DMWT is ideal with different intense loads interconnection with TTSCCTL.

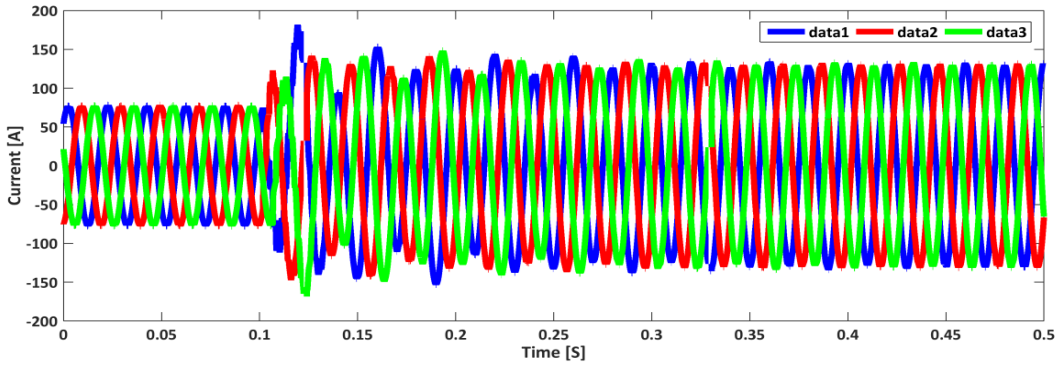

Fig. 19. Current waveform during heavy load interconnection at 0.1 s and 200 km (at bus-2) with P=550 MW and Q=350 MVAr.

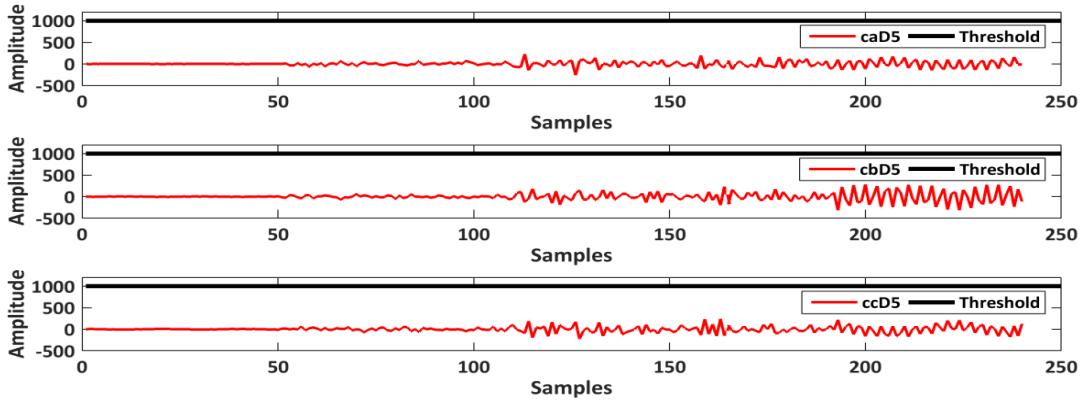

Fig. 20. DMWT coefficients during heavy load interconnection at 0.1 s and 200 km (at bus-2) with P=550 MW and Q=350 MVAr.

Table 9. Effectiveness of DMWT in detecting faults during interconnection of different types of intense loads.

Load active power [MW]	Load reactive power [MVAr]	FST [s]	Fault location [km]	DMWT output				Relay output
				Phase-A	Phase-B	Phase-C	Ground	
550	350	0.1	200	226.6244	286.3461	238.4120	4.4966*10^-5	No-Fault
850	650	0.2	200	173.1441	266.0529	424.7097	6.5462*10^-4	No-Fault
1050	850	0.3	200	196.2230	207.4765	244.4558	5.0123*10^-5	No-Fault

4.10. Effectiveness of DMWT in Detecting Faults with Various TTSCCTL Source Frequency

Efficacy of DMWT has been checked for variations in the source frequency of TTSCCTL. Fig. 21 depicts the three-phase currents; and the DMWT coefficients are shown in Fig. 22. BG fault (Fig. 21 shows the three-phase fault currents) has been simulated at 0.05 s with F_S=48 Hz, R_F = 2.5 Ω and R_G = 3.5 Ω at 135 km. Fig. 22 shows the output of fault recognition wherein the DMWT coefficients of phase-B exceeds the threshold at sample#140, while that of phase A and C are below the threshold. This - without a doubt – point out to the incidence of BG fault on TTSCCTL. The selected fault factors – which are common for all of the fault cases - are: FST = 0.05 s, F_L=135 km, R_F = 2.5 Ω and R_G = 3.5 Ω. Table 10 reports the results - of the test studies for different faults with variation in the source frequency - that consent the successful performance of DMWT in detecting faults and categorizing the faulty phases.

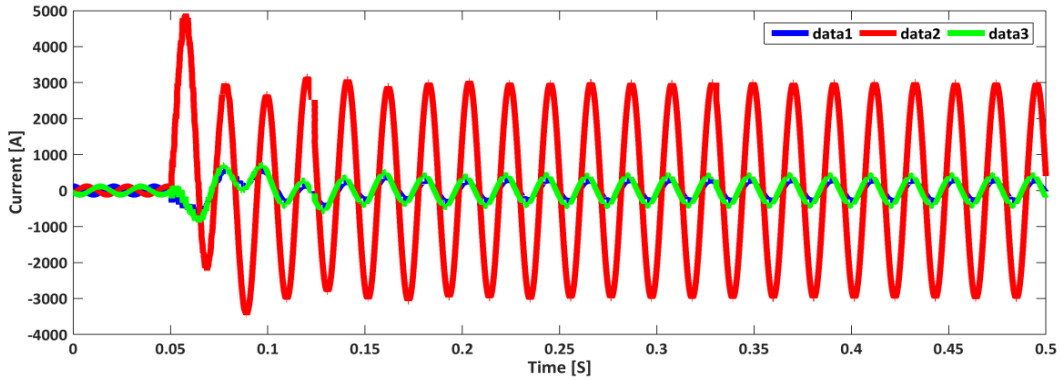

Fig. 21. BG fault at 0.05 s and 135 km with R_F = 2.5 Ω, R_G = 3.5 Ω and F_S=48 Hz.

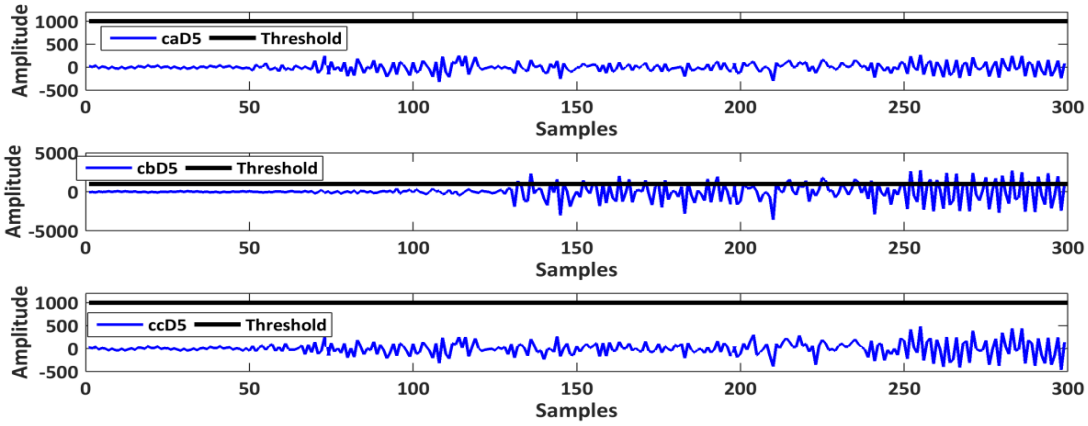

Fig. 22. DMWT coefficients for BG fault at 0.05 s and 135 km with R_F = 2.5 Ω, R_G = 3.5 Ω and F_S=48 Hz.

Table 10. Effectiveness of DMWT in detecting faults with various TTSCCTL frequencies.

F_T	F [Hz]	R_F [Ω]	R_G [Ω]	FST [s]	F_L [km]	DMWT output				O/P
						Phase-A	Phase-B	Phase-C	Ground	
BG	48	2.5	3.5	0.05	135	270.3263	2.7574*10^3	486.2761	1.1713*10^3	BG
AC	49	2.5	3.5	0.05	135	6.9682*10^3	132.5284	5.7855*10^3	1.0335	AC
ABG	50.50	2.5	3.5	0.05	135	5.1514*10^3	4.2105*10^3	462.1187	556.0774	ABG
ABC	51	2.5	3.5	0.05	135	5.1430*10^3	4.8267*10^3	4.2753*10^3	121.3685	ABC
BCG	52	2.5	3.5	0.05	135	386.8717	4.4138*10^3	5.5432*10^3	553.7347	BCG

4.11. Effectiveness of DMWT in Detecting Intermittent Faults

Efficacy of DMWT has been validated for detecting the intermittent faults. Fig. 23 shows the three-phase currents, whereas the DMWT outputs are shown in Fig. 24. The ABCG fault has been switched on at T=0.05 s and the fault has been switched off at T=0.2 s with R_F = 2.25 Ω and R_G = 3.15 Ω at 85 km. Fig. 24 shows the output of fault recognition technique wherein the DMWT outputs of all the three phases exceeds the threshold at sample#80 (phase-A), sample#75 (phase-B) and sample#75 (phase-C); pointing out - without a doubt - to the incidence of ABCG fault on TTSCCTL. The selected fault inputs – which are common for all the fault cases - are: R_F = 2.25 Ω and R_G = 3.15 Ω. Table 11 details the outcomes of the test studies for different intermittent faults with different fault types, fault time and fault locations. Hence, the simulation results approve the successful performance of DMWT in recognizing the intermittent faults and categorizing the faulty phases. Table 12 shows a comparison between the proposed DMWT-based technique and other reported techniques in detecting different fault types, locations, resistances, frequencies, and switching times.

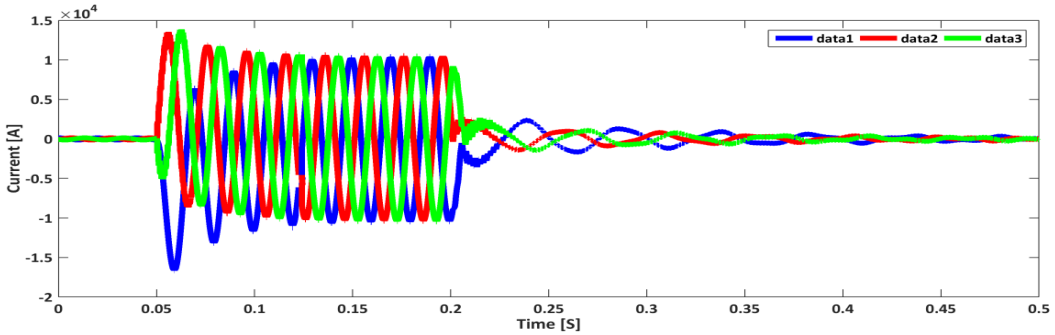

Fig. 23. ABCG fault at T = [0.05-0.2] s and 85 km with R_F = 2.25 Ω and R_G = 3.15 Ω.

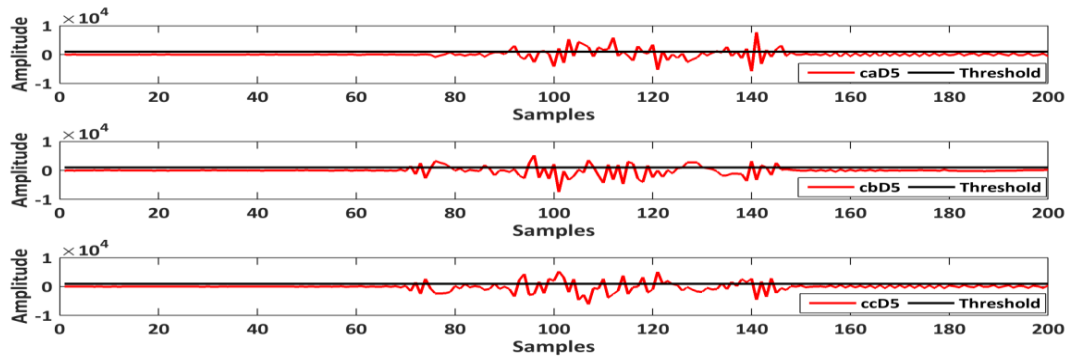

Fig. 24. DMWT coefficients for ABCG fault at T = [0.05-0.2] s and 85 km with R_F = 2.25 Ω and R_G = 3.15 Ω.

Table 11. Effectiveness of DMWT in detecting intermittent faults.

F_T	FST [s]	FET [s]	R_F [Ω]	R_G [Ω]	F_L [km]	DMWT output				O/P
						Phase-A	Phase-B	Phase-C	Ground	
ABCG	0.05	0.2	2.25	3.15	85	7.7213*10^3	5.3269*10^3	5.2969*10^3	970.1572	ABCG
AB	0.1	0.25	2.25	3.15	100	9.7914*10^3	1.0204*10^4	234.1486	0.0911	AB
BC	0.15	0.3	2.25	3.15	120	130.9469	5.8379*10^3	5.0127*10^3	0.4889	BC
AG	0.2	0.35	2.25	3.15	70	8.3595*10^3	872.0593	872.7337	3.1427*10^3	AG
ABC	0.1	0.25	2.25	3.15	130	4.0797*10^3	5.0884*10^3	4.2591*10^3	84.3051	ABC

Table 12. Comparison between the proposed DMWT-based technique and other reported techniques in detecting various types of faults.

Parameters	Proposed work	Reference [1]	Reference [11]	Reference [12]	Reference [13]
Algorithm used	Discrete Meyer Wavelet transform	Discrete Fourier Transform+ Fuzzy logic	Decision Tree +Travelling Wave	Differential Power Protection	Variational Mode Decomposition +Random Vector Functional Link Network
Input signals used	3-phase single-side currents	3-phase single-side current and voltage	3-phase single-side current and voltage	Not mentioned	3-phase single-side currents
No-fault situation reported	Yes	No	No	No	No
Ground fault detection	Yes	Yes	No	No	No
Fault resistance	0.5 Ω-105 Ω	0.001 Ω-100 Ω	10 Ω-100 Ω	10 Ω-600 Ω	10 Ω-200 Ω
Fault type	Yes	Yes	Yes	Yes	Yes
Fault location	Yes	Yes	Yes	Yes	Yes
Ground resistance	Yes	No	No	No	No
Close-in relay faults	Yes (5 km- to 9 km)	No	Yes	No	No
Far-end relay faults	Yes (195 km- 199 km)	No	Yes	No	No
Fault switching time/ FIA	Yes	Yes	FIA (0°, 90°)	FIA (0°-90°)	FIA (18°-120°)
Evolving fault reported	Yes	Yes	No	No	No
Series compensation level variation	Yes (15%- 70%)	Yes (10%- 65%)	No	No	Yes (25%- 65%)
Source frequency variation	Yes (48 Hz-52 Hz)	Yes (58 Hz- 62 Hz)	No	No	No
Faults around capacitors	Yes (Both before and after)	No	No	No	No
Intense load interconnection	Yes	Yes	No	No	No
Ungrounded faults reported	Yes	Yes	Yes	Yes	Yes
Switching events considered	Yes	Yes	No	No	No
Intermittent faults	Yes	No	No	No	No

5. CONCLUSIONS

This work presented an improved revelation using DMWT to identify and categorize faults occurring on three-phase series compensated transmission lines. The DMWT coefficients of the three-phase currents of the TTSCCTL, measured at one-end, were employed by DMWT for fault detection, categorization and faulty phase recognition. The variation in fault type included different types of grounded and ungrounded faults and the value of fault resistance was varied from 0.5 Ω to 105 Ω, the position of fault for the close-in relay faults was varied from 5 km to 9 km, the position of fault for the far-end relay faults was varied from 195 km to 199 km, the position of fault around the bank of series capacitors were changed and the degree of series compensation was also varied from 15% to 70%. Moreover, the performance of DMWT was investigated for intense loads' interconnection and the frequency of TTSCCTL was varied from 48 Hz to 52 Hz. The simulation results support the evenness of DMWT under extensive variations in fault type, location, resistance, frequency and switching time. It was also noticeable that there is an evident intolerance between the fault and no-fault situations, which establishes the potential of the DMWT-based fault recognition and faulty phase categorization technique for recognizing the faults correctly.

REFERENCES

[1] P. Mishra, A. Yadav, "Combined DFT and fuzzy based faulty phase selection and classification in a series compensated transmission line," *Modelling and Simulation in Engineering*, vol. 2019, pp. 1-18, 2019.

[2] V. Ashok, A. Yadav, "A real-time fault detection and classification algorithm for transmission line faults based on MODWT during power swing," *International Transactions on Electrical Energy Systems*, vol. 30, no. 1, pp. 1-27, 2020.

[3] A. Ameli, A. Hooshyar, E. El-Saadany, A. Youssef, "An intrusion detection method for line current differential relays," *IEEE Transactions on Information Forensics and Security*, vol. 15, pp. 329-344, 2019.

[4] B. Chaitanya, A. Yadav, M. Pazoki, "An improved differential protection scheme for micro-grid using time frequency transform," *Electrical Power and Energy Systems*, vol. 111, pp. 132-143, 2019.

[5] R. Kumar, O. Mahela, M. Kumar, N. Suyan, N. Kumar, "A current based algorithm using harmonic wavelet transform and rule based decision tree for transmission line protection," *Proceedings of IEEE 4th International Conference on Internet of Things: Smart Innovation and Usages*, pp. 1-3, 2019.

[6] M. Manohar, E. Koley, S. Ghosh, "Enhancing resilience of PV-fed microgrid by improved relaying and differentiating between inverter faults and distribution line faults," *Electrical Power and Energy Systems*, vol. 108, pp. 271-279, 2019.

[7] J. Matarweh, R. Mustaklem, A. Saleem, O. Mohamed, "The application of discrete wavelet transform to classification of power transmission system faults," *Proceedings of the IEEE Jordan International Joint Conference on Electrical Engineering and Information Technology*, pp. 699-704, 2019.

[8] S. Shukla, E. Koley, S. Ghosh, "DC offset estimation-based fault detection in transmission line during power swing using ensemble of decision tree," *IET Science, Measurement and Technology*, vol. 13, no. 2, pp. 212-222, 2019.

[9] R. Nanda, D. Bisoi, A. Behera, B. Panigrahi, A. Satapathy, "Classification of faults in a wind connected power system using artificial neural network," *Proceedings of 3rd IEEE International Conference on Computing Methodologies and Communication*, pp. 504-507, 2019.

[10] B. Chaitanya, A. Soni, A. Yadav, "Communication assisted fuzzy based adaptive protective relaying scheme for microgrid," *Journal of Power Technologies*, vol. 98, no. 1, pp. 57-69, 2018.

[11] B. Chaitanya, A. Yadav, "Decision tree aided travelling wave based fault section identification and location scheme for multi-terminal transmission lines," *Measurement*, vol. 135, pp. 312-322, 2019.

[12] M. Kundu, S. Debnath, "High impedance fault classification in UPFC compensated double circuit transmission lines using differential power protection scheme," *Proceedings of 2018 IEEE International Conference on Applied Signal Processing Conference*, pp. 54-58, 2018.

[13] M. Sahani, P. Dash, "Fault location estimation for series-compensated double-circuit transmission line using parameter optimized variational mode decomposition and weighted P-norm random vector functional link network," *Applied Soft Computing Journal*, vol. 85, pp. 1-18, 2019.